AD-A172 703 FEASIBILITY OF MEASURING RUBY LUMINESCENCE WAVELENGTH SHIFT UNDER SHOCK L (U) WASHINGTON STATE UNIV PULLMAN SHOCK DYNAMICS LAB P HORN ET AL 01 SEP 85 1/1

UNCLASSIFIED WSU-SDL-127-FTR DNA-TR-85-392 F/G 20/11 NL

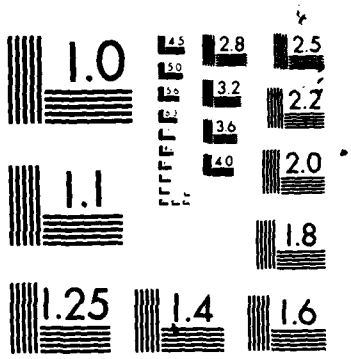

MICROCOPY RESOLUTION TEST CHART
NATIONAL BUREAU OF STANDARDS-1963-A

AD-A172 703

(12)

DNA-TR-85-392

FEASIBILITY OF MEASURING RUBY LUMINESCENCE WAVELENGTH SHIFT UNDER SHOCK LOADING

P. Horn
Y. M. Gupta
G. E. Duvall
Washington State University
Department of Physics
Shock Dynamics Laboratory
Pullman, WA 99164-2814

DTIC
ELECTE
OCT 1 4 1986
S D
D

1 September 1985

Technical Report

CONTRACT No. DNA 001-84-C-0179

Approved for public release;
distribution is unlimited.

THIS WORK WAS SPONSORED BY THE DEFENSE NUCLEAR AGENCY
UNDER RDT&E RMSS CODE B345085466 J11AMXJI00039 H2590D.

Prepared for
Director
DEFENSE NUCLEAR AGENCY
Washington, DC 20305-1000

DTIC FILE COPY

86 10 9 003

Destroy this report when it is no longer needed. Do not return to sender.

PLEASE NOTIFY THE DEFENSE NUCLEAR AGENCY, ATTN: STTI, WASHINGTON, DC 20305-1000, IF YOUR ADDRESS IS INCORRECT, IF YOU WISH IT DELETED FROM THE DISTRIBUTION LIST, OR IF THE ADDRESSEE IS NO LONGER EMPLOYED BY YOUR ORGANIZATION.

DNA PRINTING PLANT

DISTRIBUTION LIST UPDATE

This mailer is provided to enable DNA to maintain current distribution lists for reports. We would appreciate your providing the requested information.

☐ Add the individual listed to your distribution list.

☐ Delete the cited organization/individual.

☐ Change of address.

NAME: _____

ORGANIZATION: _____

OLD ADDRESS	CURRENT ADDRESS
_____	_____
_____	_____
_____	_____

TELEPHONE NUMBER: ( ) _____

SUBJECT AREA(s) OF INTEREST:

_____ _____

_____ _____

_____ _____

DNA OR OTHER GOVERNMENT CONTRACT NUMBER: _____

CERTIFICATION OF NEED-TO-KNOW BY GOVERNMENT SPONSOR (if other than DNA):

SPONSORING ORGANIZATION: _____

CONTRACTING OFFICER OR REPRESENTATIVE: _____

SIGNATURE: _____

Director
Defense Nuclear Agency
ATTN: STTI
Washington, DC 20305-1000

Director
Defense Nuclear Agency
ATTN: STTI
Washington, DC 20305-1000

UNCLASSIFIED
SECURITY CLASSIFICATION OF THIS PAGE

AD-A172 703

REPORT DOCUMENTATION PAGE

Form Approved
OMB No. 0704-0188
Exp. Date: Jun 30, 1986

1a REPORT SECURITY CLASSIFICATION UNCLASSIFIED	1b RESTRICTIVE MARKINGS
2a SECURITY CLASSIFICATION AUTHORITY N/A since Unclassified 2b DECLASSIFICATION/DOWNGRADING SCHEDULE N/A since Unclassified	3 DISTRIBUTION/AVAILABILITY OF REPORT Approved for public release; distribution is unlimited
4 PERFORMING ORGANIZATION REPORT NUMBER(S) SDL-127 FTR	5 MONITORING ORGANIZATION REPORT NUMBER(S) DNA-TR-85-392
6a NAME OF PERFORMING ORGANIZATION Washington State University Department of Physics, SDL 6b OFFICE SYMBOL (If applicable)	7a NAME OF MONITORING ORGANIZATION Director Defense Nuclear Agency
6c ADDRESS (City, State, and ZIP Code) Pullman, WA 99164-2814	7b ADDRESS (City, State, and ZIP Code) Washington, DC 20305-1000
8a NAME OF FUNDING SPONSORING ORGANIZATION 8b OFFICE SYMBOL (If applicable)	9 PROCUREMENT INSTRUMENT IDENTIFICATION NUMBER DNA 001-84-C-0179
8c ADDRESS (City, State, and ZIP Code)	10 SOURCE OF FUNDING NUMBERS PROGRAM ELEMENT NO: 62715H; PROJECT NO: J11AMXJ; TASK NO: I; WORK UNIT ACCESSION NO: DH008309

11 TITLE (Include Security Classification)
FEASIBILITY OF MEASURING RUBY LUMINESCENCE WAVELENGTH SHIFT UNDER SHOCK LOADING

12 PERSONAL AUTHOR(S)
Horn, P.; Gupta, Y.M.; and Duvall, G.E.

13a TYPE OF REPORT	13b TIME COVERED	14 DATE OF REPORT (Year, Month, Day)	15 PAGE COUNT
Technical	FROM 840301 TO 850401	850901	52

16 SUPPLEMENTARY NOTATION
This work was sponsored by the Defense Nuclear Agency under RDT&E RMSS Code B345085466 J11AMXJI00039 H2590D.

17 COSATI CODES			18 SUBJECT TERMS (Continue on reverse if necessary and identify by block number)
FIELD	GROUP	SUB-GROUP	Ruby Luminescence, Shock, Shock Wave, Ruby Fluorescence, Transducer, High Pressure, R-Lines
20	6		
20	5		

19 ABSTRACT (Continue on reverse if necessary and identify by block number)

The feasibility of developing an optical stress transducer and transmission system for use under dynamic loading is described. The ruby luminescence (R-lines) wavelength shift was selected as the conceptual basis for dynamic stress measurements. An experimental configuration using thin ruby crystals as transducers and optical fibers for signal transmission in plate impact experiments was developed. Calculations pertinent to generation and collection of luminescence are presented. Impact experiments using photomultiplier tubes and an optical multichannel analyzer as detectors were performed to examine the validity of the experimental design. Results of these preliminary experiments show a shift in the luminescence R-lines, as expected. Although the present results demonstrate the feasibility of developing an optical stress transducer, further research efforts are needed before time-resolved quantitative measurements can be obtained. Future experiments are outlined. Spectral transmission characteristics of shocked optical fibers have also been resolved.

20 DISTRIBUTION/AVAILABILITY OF ABSTRACT ☐ UNCLASSIFIED/UNLIMITED ☒ SAME AS RPT ☐ DTIC USERS	21 ABSTRACT SECURITY CLASSIFICATION UNCLASSIFIED
22a NAME OF RESPONSIBLE INDIVIDUAL Betty L. Fox	22b TELEPHONE (Include Area Code) (202) 325-7042 22c OFFICE SYMBOL DNA/STTI

DD FORM 1473, 84 MAR — 83 APR edition may be used until exhausted. All other editions are obsolete.

SECURITY CLASSIFICATION OF THIS PAGE
UNCLASSIFIED

SUMMARY

The feasibility of using the wavelength shift of the ruby luminescence R-lines to measure stresses under dynamic loading was examined in the present work. Our objective was to design and develop an experimental method that would permit us to monitor the wavelength of the R-lines in well-defined plate impact experiments.

The first stage of our work involved a detailed examination of the existing results on the ruby spectrum under static high-pressure conditions, as well as the effects of temperature. We concluded that unambiguous interpretation of ruby spectra under shock loading would require the R1 (694.3 nm) and R2 (692.9 nm) spectral lines to be resolved. Also, because the temperature induced wavelength shift effectively ceases below 100 K, it may be possible to separate temperature and stress effects by performing low temperature experiments.

The experimental design, including excitation and detection of the ruby spectrum, was a consequence of the different characteristic times involved in the problem. The lifetime of the ruby luminescence is approximately 3 ms, while the times of interest in our shock experiments are typically less than 1 μs. Because of this, we have chosen an "evolutionary" approach to recording the spectrum wherein the ruby is excited by a cw Argon laser, and the spectrum is recorded continuously as it evolves in time. Calculations of the luminescence excitation and collection were performed and experimentally verified at different stages of the experimental assembly to develop the experimental configuration used in the impact experiments.

Several experiments were performed to verify that the wavelength shift is observable on a relevant time frame. Very thin ruby disks (approximately 62 μm thick) were shocked, and the luminescence spectrum was recorded in two different ways. In the first set of experiments, luminescence from each ruby R-line was transmitted from the focal plane of a spectrometer to a photomultiplier tube by an optical fiber. The photomultiplier signals showed changes indicative of a wavelength shift, coinciding with the arrival of the shock wave at the

thin ruby disks, and occuring within the risetime of the electronics. Further experiments were done in which the spectrum was recorded at 144 ns intervals by a streak camera and an optical multichannel analyzer with a Vidicon detector. These records also indicated a wavelength shift under shock loading. Based on these results, we believe that it is feasible to measure the stress induced wavelength shift on a 10-50 ns timescale.

The signal levels obtained in our preliminary experiments were insufficiently strong to allow resolution of the R-lines. A number of modifications in the optical system are discussed which would remedy this. Among these is the placement of an optical fiber in direct contact with the shocked ruby sample. Before implementing this, we performed experiments to determine if changes would occur in the fiber transmission spectrum under shock loading. We found that under conditions identical to those in the luminescence experiments, hard-clad silica fibers, bonded into silica or PMMA supports, showed no change in transmission in the spectral range 345-649 nm over a 1 μs period after shocking the fiber face. This corresponded to the time for the shock to propagate to the back of the supporting medium. An experiment with sapphire fiber gave similar results.

With the completion of the modifications mentioned above, it should be possible to obtain ruby spectra with sufficient temporal and spectral resolution to make quantitative measurements of the wavelength shift. Making these measurements on z-cut ruby samples at ambient and low temperatures should provide an opportunity to understand the stress-induced wavelength shift on an atomic scale, to compare static and dynamic high-pressure data, and to separate temperature and pressure effects. An understanding of these phenomena is important for using the ruby luminescence shift as an accurate stress transducer under dynamic loading.

PREFACE

This report describes research sponsored by DNA under Contract 001-84-C-0179. The project was monitored by Dr. M. J. Frankel. His interest and enthusiastic support are sincerely acknowledged.

The authors are grateful to the following individuals for their contributions: Scientific discussions with Dr. M. J. Frankel, Dr. T. Hirschfeld (Lawrence Livermore Laboratory), and Professor P. F. Braunlich (Washington State University) were very helpful in the initial stages of this work. The static pressure and temperature studies by Dr. Hirschfeld and co-workers, and related discussions were valuable to our effort. Professor Braunlich's considerable expertise on lasers and optical measurements, and his willingness to critique our ideas was extremely helpful. He is also thanked for loaning us several pieces of equipment from his laboratory. The assistance of P. Bellamy, J. Thompson, and J. Burt with the experimental effort is acknowledged.

CONVERSION TABLE

Conversion factors for U.S. customary to metric (SI) units of measurement.

To Convert From	To	Multiply By
angstrom	meters (m)	1.000 000 X E -10
atmosphere (normal)	kilo pascal (kPa)	1.013 25 X E +2
bar	kilo pascal (kPa)	1.000 000 X E +2
barn	meter^2 (m^2)	1.000 000 X E -28
British thermal unit (thermochemical)	joule (J)	1.054 350 X E +3
cal (thermochemical)/cm^2§	mega joule/m^2 (MJ/m^2)	4.184 000 X E -2
calorie (thermochemical)§	joule (J)	4.184 000
calorie (thermochemical)/g§	joule per kilogram (J/kg)*	4.184 000 X E +3
curie§	giga becquerel (GBq)†	3.700 000 X E +1
degree Celsius‡	degree kelvin (K)	$t_K = t°_C + 273.15$
degree (angle)	radian (rad)	1.745 329 X E -2
degree Fahrenheit	degree kelvin (K)	$t_K = (t°_F + 459.67)/1.8$
electron volt§	joule (J)	1.602 19 X E -19
erg§	joule (J)	1.000 000 X E -7
erg/second	watt (W)	1.000 000 X E -7
foot	meter (m)	3.048 000 X E -1
foot-pound-force	joule (J)	1.355 818
gallon (U.S. liquid)	meter^3 (m^3)	3.785 412 X E -3
inch	meter (m)	2.540 000 X E -2
jerk	joule (J)	1.000 000 X E +9
joule/kilogram (J/kg) (radiation dose absorbed)§	gray (Gy)*	1.000 000
kilotons§	terajoules	4.183
kip (1000 lbf)	newton (N)	4.448 222 X E +3
kip/inch^2 (ksi)	kilo pascal (kPa)	6.894 757 X E +3
ktap	newton-second/m^2 (N-s/m^2)	1.000 000 X E +2
micron	meter (m)	1.000 000 X E -6
mil	meter (m)	2.540 000 X E -5
mile (international)	meter (m)	1.609 344 X E +3
ounce	kilogram (kg)	2.834 952 X E -2
pound-force (lbf avoirdupois)	newton (N)	4.448 222
pound-force inch	newton-meter (N•m)	1.129 848 X E -1
pound-force/inch	newton/meter (N/m)	1.751 268 X E +2
pound-force/foot^2	kilo pascal (kPa)	4.788 026 X E -2
pound-force/inch^2 (psi)	kilo pascal (kPa)	6.894 757
pound-mass (lbm avoirdupois)	kilogram (kg)	4.535 924 X E -1
pound-mass-foot^2 (moment of inertia)	kilogram-meter^2 (kg•m^2)	4.214 011 X E -2
pound-mass/foot^3	kilogram-meter^3 (kg/m^3)	1.601 846 X E +1
rad (radiation dose absorbed)§	gray (Gy)*	1.000 000 X E -2
roentgen§	coulomb/kilogram (C/kg)	2.579 760 X E -4
shake	second (s)	1.000 000 X E -8
slug	kilogram (kg)	1.459 390 X E +1
torr (mm Hg, 0° C)	kilo pascal (kPa)	1.333 22 X E -1

*The gray (Gy) is the accepted SI unit equivalent to the energy imparted by ionizing radiation to a mass of energy corresponding to one joule/kilogram.
†The becquerel (Bq) is the SI unit of radioactivity; 1 Bq = 1 event/s
‡Temperature may be reported in degree Celsius as well as degree kelvin
§These units should not be converted in DNA technical reports; however, a parenthetical conversion is permitted at the author's discretion.

TABLE OF CONTENTS

Section	Page
SUMMARY	iii
PREFACE	v
CONVERSION TABLE	vi
LIST OF ILLUSTRATIONS	viii
1 INTRODUCTION	1
1.1 Objectives	1
1.2 Background on Ruby Luminescence	2
1.2.1 Stress Related Spectral Changes	2
1.2.2 Temperature Related Spectral Changes	4
1.3 Applicability to Shock Wave Experiments	4
2 EXPERIMENTAL METHOD AND RESULTS	7
2.1 Experimental Configuration	7
2.1.1 Sensor Configuration	7
2.1.2 Target Preparation and Configuration	8
2.1.3 Experimental Layout for Detection	8
2.2 Shock Experiments	12
2.2.1 Photomultiplier Detection	12
2.2.2 Photomultiplier Results	15
2.2.3 Streak Camera Recording	18
2.2.4 Streak Camera Results	19
3 DISCUSSION	23
3.1 Apparatus Improvements	23
3.2 Shock Loading of Optical Fiber	24
3.3 Conclusion	25
4 LIST OF REFERENCES	26
APPENDIX	27
A.1 Luminescence Power Calculation	27
A.2 Fluorescence Collection	34
A.2.1 Fiber Collection Efficiency	34
A.2.2 Spectrometer Collection Efficiency	35
A.2.3 System Collection Efficiency	37

QUALITY INSPECTED 4

Accesion For
NTIS CRA&I ☑
DTIC TAB ☐
Unannounced ☐
Justification
By
Distribution /
Availability Codes
Dist | Avail and / or Special
A-1

LIST OF ILLUSTRATIONS

Figure		Page
1	Energy Level Diagram for Ruby	3
2	Ruby R-Line Spectra at Various Static High Pressures [2]	6
3	Shock Target Cross Sectional View	9
4	Shock Target Front View	10
5	Optical Layout	11
6	Details of Photomultiplier Recording Apparatus	13
7	Oscilloscope Record of Photomultiplier Signal	16
8	Oscilloscope Record of Photomultiplier Signal During Shocking of Ruby Sample	17
9	Compressed Plot of OMA Data Showing Ruby Spectra During a Shock Experiment	20
10	Expanded Plot of 5 Ruby Spectra During a Shock Experiment	21
11	Diagram of Geometry Used in the Calculation of Luminescence Generation	28

SECTION 1

INTRODUCTION

1.1 OBJECTIVES.

An important need for DNA programs is the ability to measure stresses under dynamic loading and to transmit this information over long distances. At present, stress measurements are obtained using either piezoresistance or piezoelectric transducers. The development of an optical stress transducer, along with the use of optical fibers to transmit this information, would be particularly attractive for experimental situations involving large electromagnetic noise. In addition, the development of such a transducer would permit an independent check on stress measurements from other transducers.

This report describes a research effort to examine the feasibility of developing an optical stress transducer and transmission system for use under dynamic loading. Specifically, the objective of the present work was to develop an experimental configuration for use with well-defined plate impact experiments. Because these experiments were the first of their kind, a considerable amount of exploratory development was involved in the present effort. We chose to examine the use of the ruby luminescence wavelength shift for stress measurements because of its use in static pressure measurements [1]. Note that the terms luminescence and fluorescence have been used interchangeably in the literature. The high mechanical strength and thermal conductivity of ruby, and the well characterized shock properties of the sapphire matrix are additional advantages for dynamic measurements. Over the stress range of interest to our present experiments, we are assuming that the mechanical properties of the ruby are identical to those of sapphire crystals.

1.2 BACKGROUND ON RUBY LUMINESCENCE.

The luminescence spectrum of ruby ($Al_2O_3:Cr^{3+}$) has been extensively studied, particularly with regard to the effects of static pressure and temperature [1,2,3,4]. As a result, the ruby spectrum is frequently used at static pressures ranging from a few kilobars to more than one megabar.

There are two ruby spectral lines of interest (the R-lines). At a pressure of one atmosphere, and room temperature, these lines have wavelengths of 694.3 nm (R1) and 692.9 nm (R2), and both have approximately 0.5 nm linewidth. Figure 1 [5] is an energy level diagram for Cr^{3+} in the sapphire lattice, showing the excitation and decay processes that lead to the R line luminescence. The chromium excited states are efficiently "pumped" by Argon laser light at 514.5 nm through an intermediate state which exhibits a very fast non-radiative decay. The luminescence then proceeds with high quantum efficiency, and has a lifetime of 3 ms at 300 K[5].

1.2.1 Stress Related Spectral Changes.

The major spectral change associated with stress is a shift in the wavelengths of the R-lines. In the case of hydrostatic pressure, the linewidth remains constant and both R lines shift toward longer wavelength at a rate of approximately 0.0365 nm/kbar [1,2,6]. Under the influence of uniaxial stress, Schawlow [7] has shown that not only do the shift rates of the R1 and R2 lines differ, but that they also depend on whether the stress is applied parallel to or perpendicular to the crystal c-axis. Considerable broadening of both lines has been observed under the influence of non-hydrostatic pressure [2,6]. Adams, et al., [2] ascribe this to the presence of multiple grains of ruby oriented in different directions, so that the wavelength shift of each grain is different. In the case where a single crystal is used, this variation with the direction of stress should lead to a change in spectral separation between R1 and R2. Even when broadening is not a problem, it is apparent that proper interpretation of the spectral data for non-hydrostatic stress requires the ability to measure the independent shifts of the R1 and R2 lines, and that the ruby crystal orientation be known. Adams,

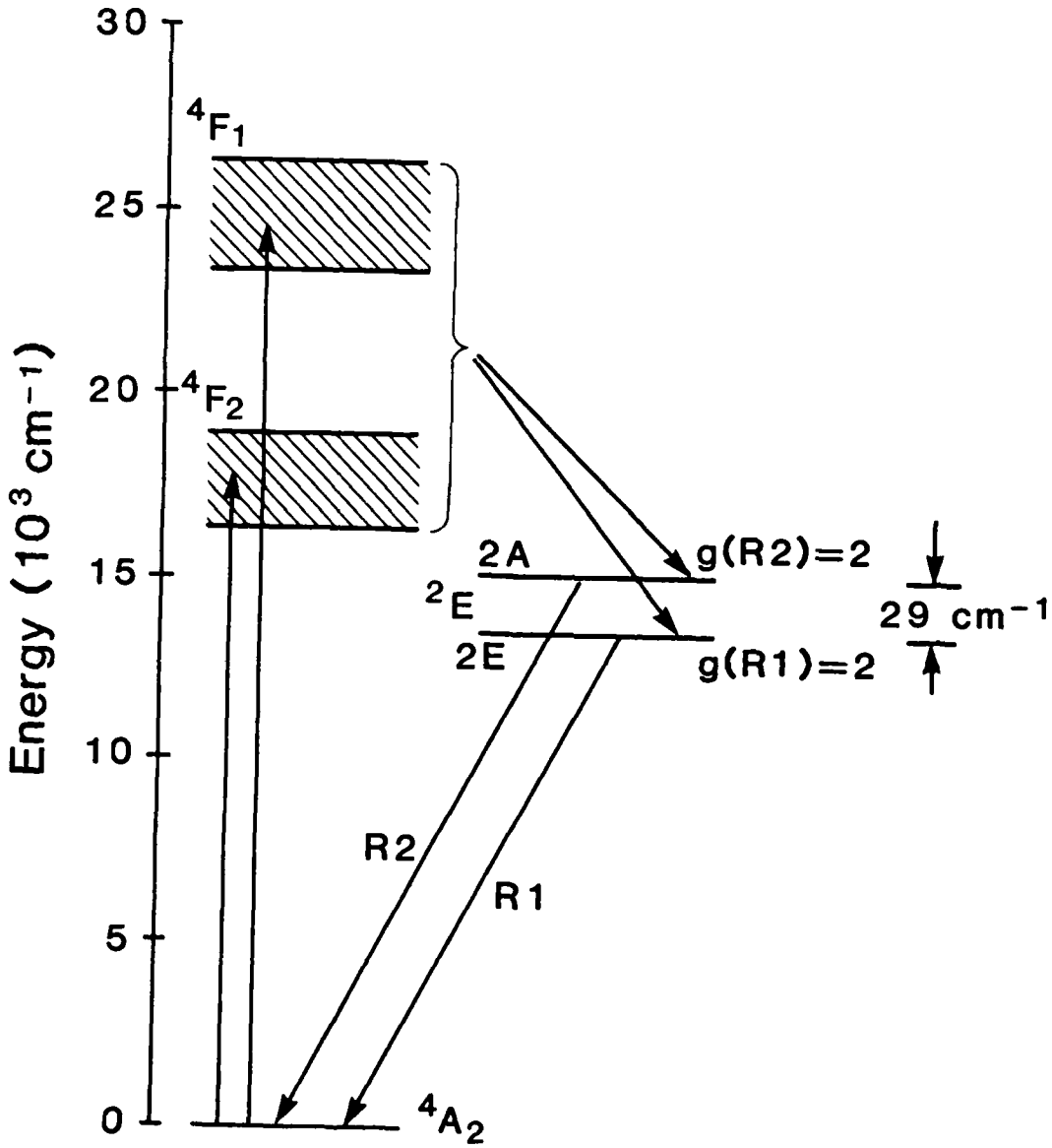

Figure 1. Energy level diagram for ruby, showing the excitation of the "pump" bands (the Argon 514,5 nm line addresses the $^4F_2$ band), the decay to the ^2E levels which are the starting point for the R-line luminescence (note that the R-line separation has been greatly exaggerated), and the decay by luminescence which generated the R-lines.

et al., [2] also state, without any explanation, that broadening may be caused by rapid pressure changes.

1.2.2 Temperature Related Spectral Changes.

The spectral variations associated with temperature include wavelength shift, broadening, varying luminescence lifetime, and a change in the ratio of the peak luminescence intensities of R1 and R2 [6]. Above 200 K, both R1 and R2 shift nearly linearly toward longer wavelength at a rate of 0.0068 nm/K [6]. This implies that the shift corresponding to a 5.4 K change is equal to that generated by a 1 kbar change in pressure. Below 100 K, there is very little wavelength shift. This feature suggests that low temperature shock wave experiments can be very useful in separating pressure and temperature effects. Above 60 K, both lines broaden roughly as the third power of the temperature [2]. The luminescence lifetime decreases with increasing temperature, but remains greater than 1 ms to above 450 K [6]. The ratio of peak intensities (R1/R2) has been shown by Hirschfeld [6] to vary with temperature. Since the R lines are energetically separated by only (1/270) eV (1/6 of kT at 300 K), this is qualitatively consistent with a thermal redistribution of electrons between the two chromium excited states.

1.3 APPLICABILITY TO SHOCK WAVE EXPERIMENTS.

In examining the applicability of the ruby luminescence technique, one must consider the characteristic stresses and temperatures generated in a typical shock experiment, as well as the time frame over which these parameters change. Since all work to date has been done under static conditions, the spectral response to time-varying stress and temperature is unknown. In our work, times of interest will typically be in the 1 ns - 1 μs range. Time resolved measurements in this range may be attempted by the following two methods. If the luminescence lifetime is much shorter than the time over which significant spectral changes occur (implying that the characteristic times for pressure and temperature changes are greater than the luminescence lifetime), a sampling technique may be applied. In this case, the ruby is excited at regular intervals, with each excitation yielding a

spectrum associated with the average conditions over the luminescence lifetime. The spectral variation from one sampling to another then traces out the temporal dependence. If, on the other hand, the luminescence lifetime is much longer than the timescale over which spectral changes occur, an "evolutionary" approach may be used. In this situation, a population of excited Cr^{3+} is created, and the "evolution" of the spectrum is observed over time as the population decays at a nearly constant rate; we plan to use this approach because the luminescence lifetime is several orders of magnitude larger than our experimental times. The use of the evolutionary approach for time-resolved stress measurements is analogous to piezoresistance gauge measurements using a constant current supply [8]. The two parameters remaining to be examined are the expected magnitudes of stress and temperature. As a start, it would be desirable to make longitudinal stress measurements in the 20-150 kbar range with approximately 1 kbar resolution. Figure 2 shows a set of spectra at various pressures as given by Adams, et al. [2]

Using the static compression shift rate of 0.0365 nm/kbar, a 1 kbar resolution requires the ability to detect a spectral shift of 0.0365 nm, which is less than 10 percent of the linewidth. At 100 kbar it would be 3.65 nm, which is greater than twice the R1-R2 separation. The temperature rise of the ruby sensor should be in the 5-50 K range (not neccessarily the same temperature increase as the shocked sample in the case where the ruby acts as a sensor in contact with another material). This would lead to a 0.034-0.34 nm shift (equivalent to 0.9-9.0 kbar) and a 5 percent to 60 percent broadening (from 300 K).

A practical problem with luminescence measurements in shock wave experiments involves collecting enough signal on the time scale of the experiments. A large fraction of the present effort was spent on addressing this problem.

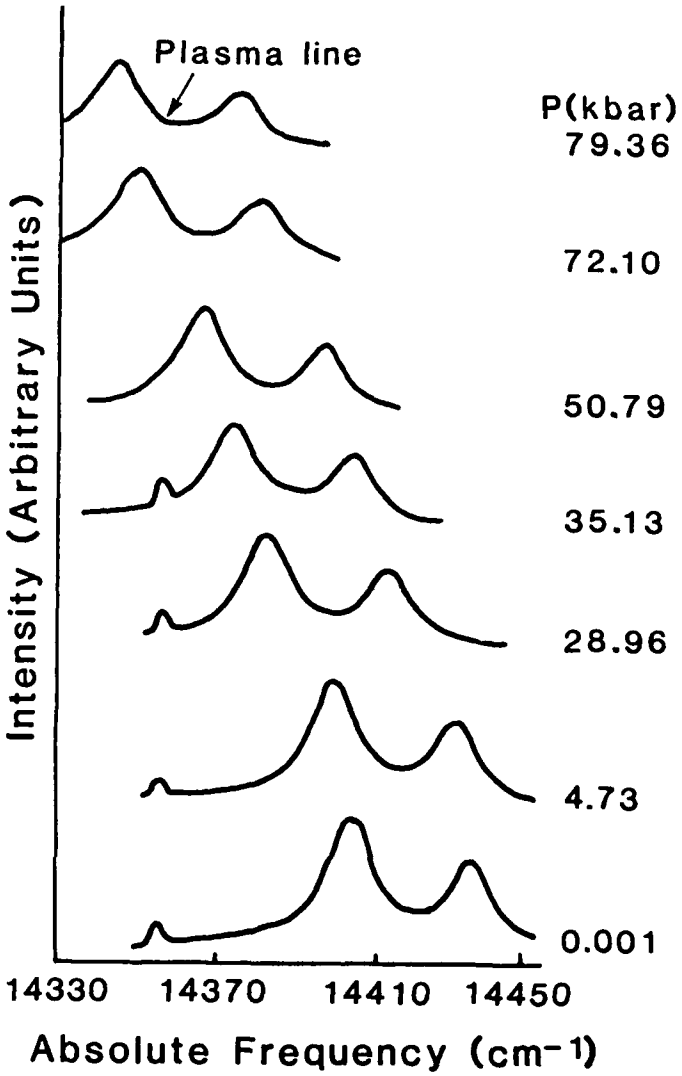

Figure 2. Ruby R-line spectra at various static high pressures [2].

SECTION 2

EXPERIMENTAL METHOD AND RESULTS

2.1 EXPERIMENTAL CONFIGURATION.

The necessary design parameters have now been defined to proceed with an examination of the possible apparatus configurations. This is most easily done by considering the system in two parts, the sensor section and the detector section, which may be separated by one or more optical fibers. The incorporation of optical fibers allows for remote placement of the detection system, which is highly desirable in shock experiments. Furthermore, very good luminescence collection efficiency can be achieved by placing the optical fiber in close proximity to the ruby sample. To aid and check the experimental design, calculations to determine the luminescence excitation and collection efficiency were performed and are presented in the Appendix.

2.1.1 Sensor Configuration.

The two choices available to us are to use a ruby sample which is separate from the optical fiber, or to dope the tip of a sapphire fiber itself with chromium. We have chosen not to use doped sapphire fibers for several reasons. First, because the rate of shift of wavelength varies with the ruby crystal orientation for the two R-lines, we would expect the ruby spectrum to be smeared in wavelength under uniaxial strain if polycrystalline fibers were used. Only recently have single crystal sapphire fibers suitable for use as optical fibers been made [9], and these are not readily available. Second, it is exceedingly difficult to obtain consistent, high chromium concentrations in a narrow region at the fiber tip, as would be required for good time resolution.

We have chosen to employ very thin, single crystal ruby disks (0.0025 inches thick, 0.5 inch diameter, 0.5% chromium by weight). In this way we obtain complete control over both the

chromium content and time resolution, as well as avoiding concerns over the effects of polycrystalline samples.

2.1.2 Target Preparation and Configuration.

The targets were constructed by pressing the thin ruby disk between two sapphire disks as shown in Figure 3. This assembly was held in the 6 inch diameter target ring by epoxy. Small brass bolts were tinned with solder and countersunk into the epoxy of the target face to provide electrical connection to a set of contacts to be vapor deposited in a later step. The entire target was then turned on a lathe so that its face was parallel to the front sapphire disk, and electrical cables were attached to the brass screws. The copper strips mentioned above were vapor deposited next as shown in Figure 4. They provided for the measurement of projectile-target tilt on impact and for the triggering of an optical timing fiducial which will be described later. A plexiglass fiber mount was then glued to the back sapphire disk with epoxy, and the polished 1 mm core fiber (Math Associates QSF-1000) was pushed into contact with the sapphire and held in place by a steel spring-clamp. Next, Argon laser light was passed through a 600 μm core fiber (QSF-600), which was then positioned to illuminate the area of ruby immediately in front of the 1 mm fiber. This was verified by observing the luminescent spot, and by measuring the luminescence power in the 1 mm fiber (using a Fotec C100A power meter). The 600 μm fiber was then attached to the plexiglass mount with epoxy. A third optical fiber (200 μm core, QSF-200) was also bonded to the plexiglass mount to carry luminescence to a photomultiplier tube (PMT) for monitoring the net luminescence without wavelength dispersion.

2.1.3 Experimental Layout for Detection.

The apparatus used in these preliminary tests is shown in Figure 5. The Argon laser light was transmitted to the gun chamber by a 0.2 mm fiber, then was coupled to a 0.6 mm fiber which illuminated the ruby sample. After each target was mounted in the gun chamber, its level of

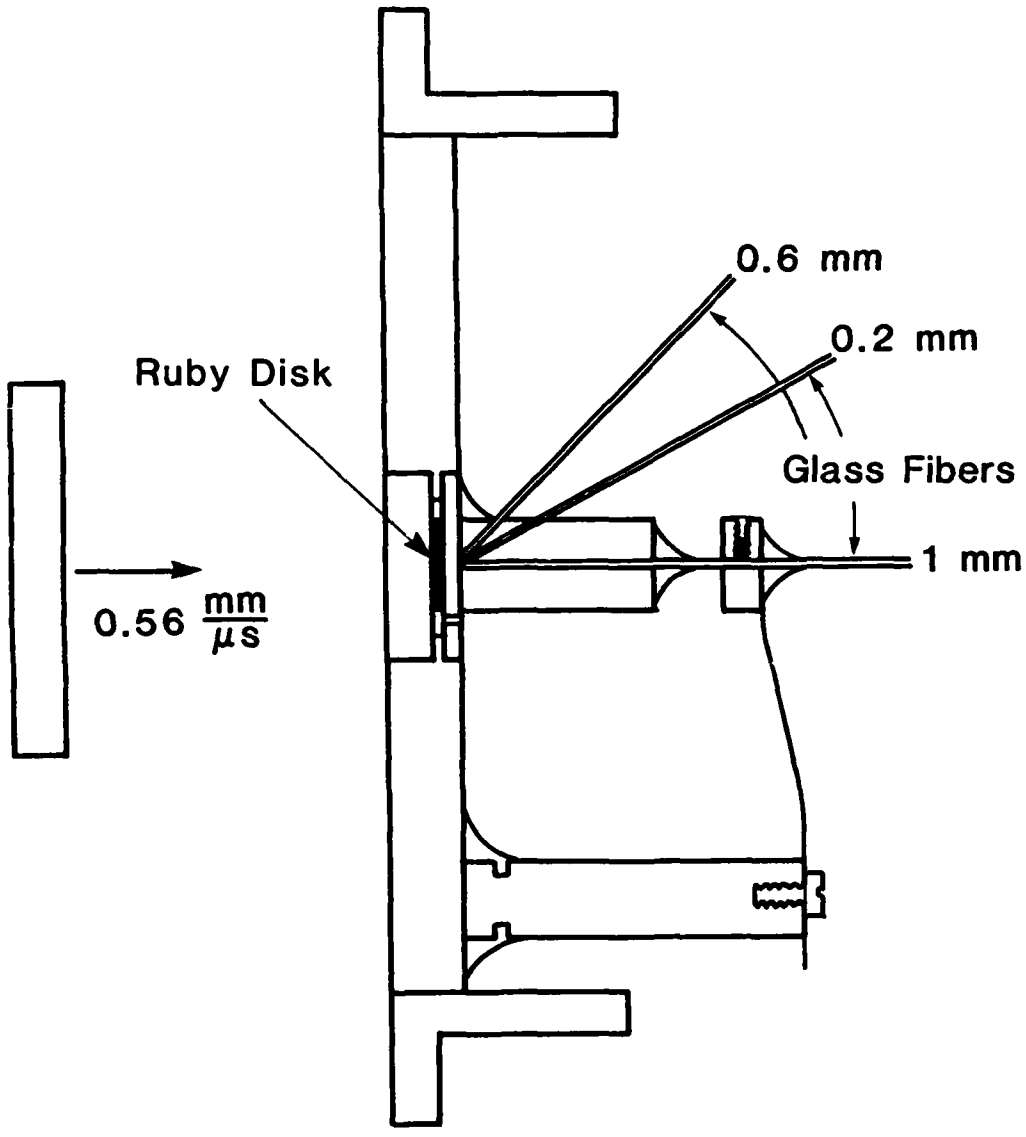

Figure 3. Shock target cross sectional view. Note that the thickness of the ruby sample is exaggerated. The Argon laser light arrives at the target via the 0.6 mm optical fiber, and luminescence is collected by the 0.2-and-1.0 mm fibers.

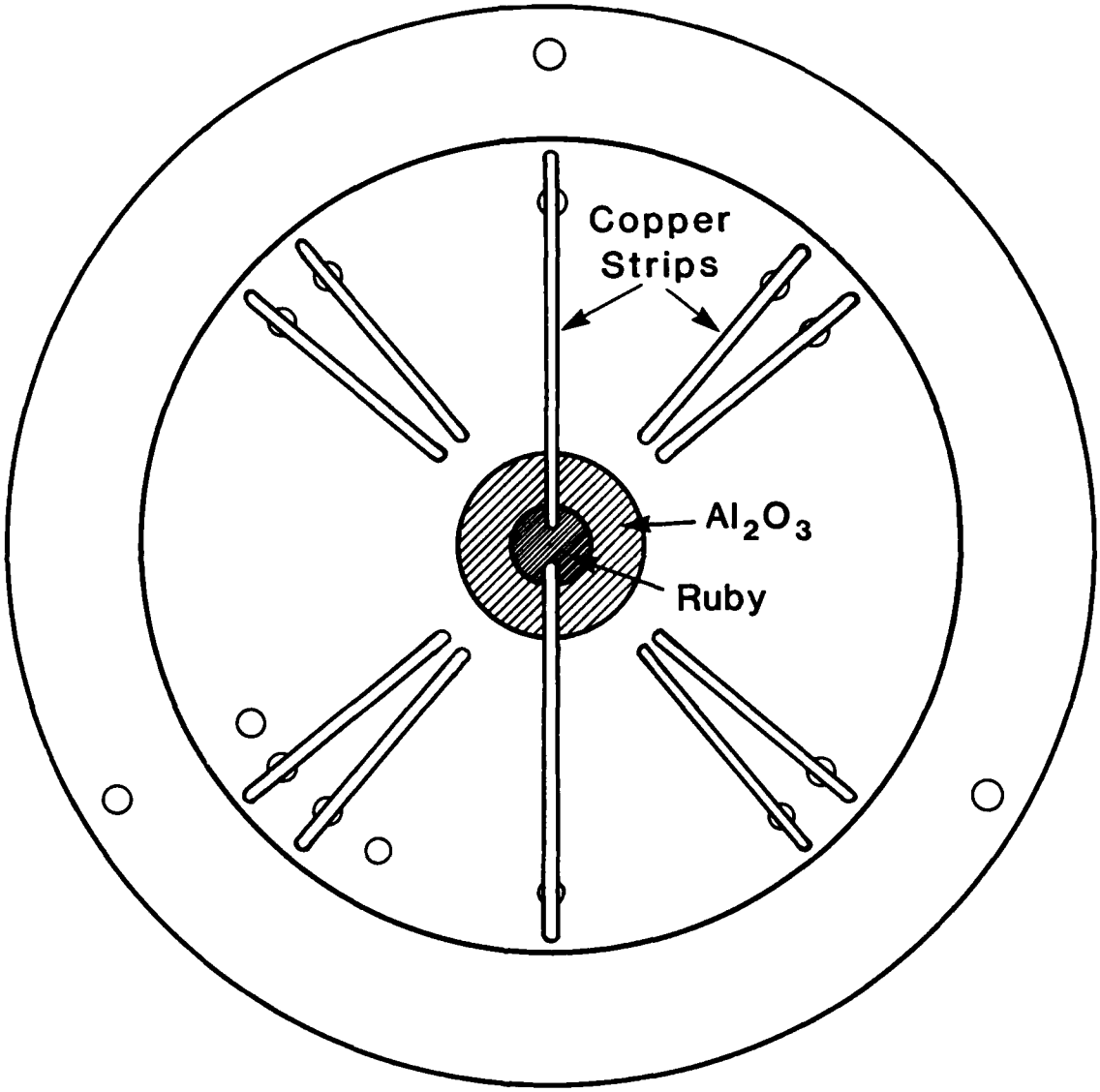

Figure 4. Shock target front view. The copper strips provide for the measurement of impactor tilt and for triggering of the optical fiducial.

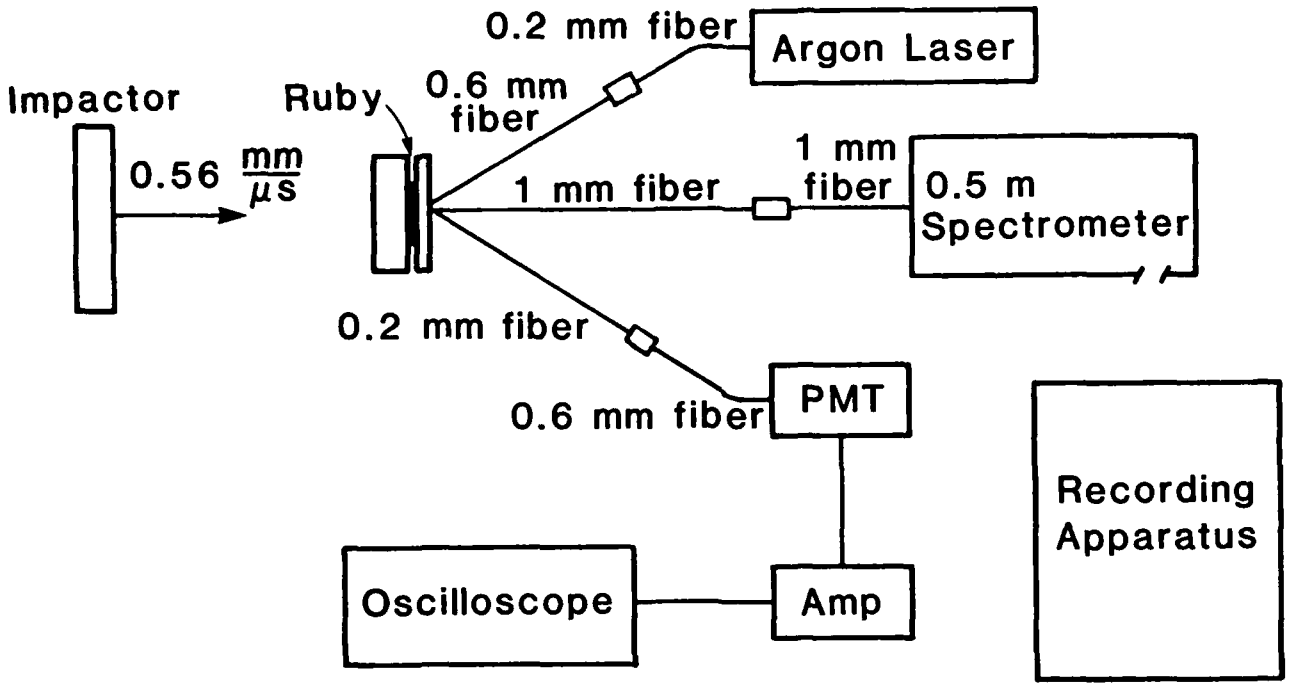

Figure 5. Optical layout. Note that the ruby thickness is exaggerated. The luminescence is excited by Argon laser light. A 0.2 mm optical fiber collects luminescence, and is coupled to a 0.6 mm fiber at the wall of the target chamber. This luminescence illuminates a photomultiplier tube to serve as a monitor for luminescence power. A 1.0 mm optical fiber transmits luminescence from the ruby sample to a 0.5 m spectrometer, and the resulting spectrum is recorded by photomultipliers or a streak camera (recording apparatus).

luminescence was tested at the 1 mm fiber. This fiber was then connected to an additional length of 1 mm fiber which delivered the luminescence directly to the entrance slit of the spectrometer. This spectrometer (0.5 m Jarrel-Ash) contained a 1180 groove/mm grating, and generated a linear dispersion of 16 A/mm. The entrance slit was opened to its maximum width of 0.4 mm, so that the 1:1 imaging in the spectrometer resulted in a spectrum consisting of the two R-lines, each 0.4 mm wide and separated by 0.88 mm at the exit "plane." Because we worked in a narrow spectral range, the field of the spectrometer was relatively flat. A third optical fiber transmitted luminescence directly to a PMT without wavelength dispersion. This served as a monitor for the luminescence power.

We considered a number of methods for recording the ruby spectrum as a function of time, including a photomultiplier array and streak camera. Both of these techniques were employed in the shock experiments and described next.

2.2 SHOCK EXPERIMENTS.

2.2.1 Photomultiplier Detection.

In our preliminary experiments, three photomultipliers (PMT) were used, each of which provided signal to a high gain current amplifier (Analog Modules, 90 MHz bandwidth, 10^5 V/A) as shown in Figure 6. Two PMTs received light input through optical fibers (QSF-600) which collected luminescence at the spectrometer exit plane. Since these fibers had a diameter of 0.6 mm, they each effectively integrated over a spectral range of 0.96 nm (due to the 1.6 nm/mm dispersion of the spectrometer). They were positioned at the locations of the R1 and R2 luminescence lines prior to the shock. Alignment of these fibers was accomplished with a five axis positioner, and tested by measuring the collected luminescence power. The third PMT received luminescence via an optical fiber (QSF-200) directly from the target (net luminescence monitor) as shown in Figure 5. All three PMTs were filtered by Corning 2-56 cutoff filters (red-pass) to eliminate stray Argon laser light.

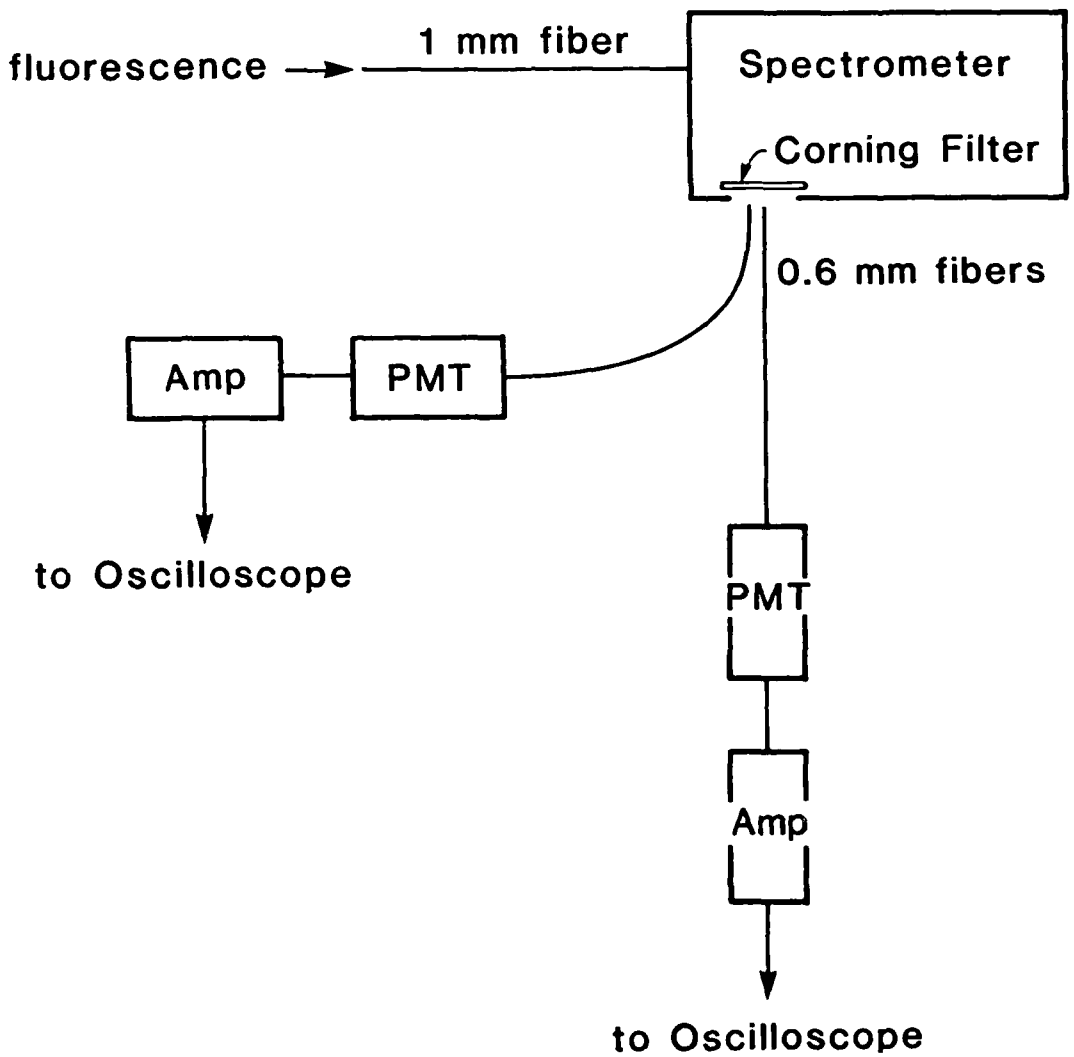

Figure 6. Details of photomultiplier recording apparatus (see Figure 5). The two 0.6 mm optical fibers are placed at the location of the R1 and R2 lines prior to shocking the ruby.

In order to correlate in time the arrival of the shock at the ruby sample and the observed spectral changes, we used a fiberoptic data transmitter (Augat model M25-T1) to generate an optical fiducial at the time of impact. This transmitter was triggered on impact by vapor deposited contacts on the target face (see Figure 4), and generated a "negative-going light pulse" (on- to off-state) of approximately 1 ms duration. This light signal was carried by an optical fiber directly to the PMT sensing the R1 luminescence line. This allowed any changes in the R1 luminescence to be correlated with impact without any knowledge of delay times in the PMT or current amplifier. All PMT signals were recorded in pairs on dual beam oscilloscopes so that any record could be traced to a correlation with the optical fiducial. Accounting for a 10 ns trigger cable delay, an 80 ns trigger circuit delay, a 200 ns fiber transit time (41.2 m of fused SiO_2 fiber), and the maximum specified data transmitter delay of 22 ns, the interval between impact and arrival of the fiducial at the PMT was 312 ns. Since our data recording took place over about 1 μs, and the PMT had a negative output, the fiducial took the form of a positive going voltage step, the magnitude of which was adjustable. In our experiments, we chose the magnitude of the fiducial to be approximately equal to the voltage step generated by chopping the ruby luminescence.

As stated previously, the PMTs were set up to record the R1 and R2 lines prior to arrival of the shock. Any shift in wavelength thus would appear on the data record as a positive voltage step (decrease in collected luminescence). The current amplifiers used were AC coupled, with a low frequency response to 120 HZ. The large bandwidth (fast response) of these amplifiers allowed for light intensity changes to be observed on a 10-50 ns scale, but also faithfully reproduced the statistical nature of the luminescence, resulting in a somewhat noisy signal. The low frequency response was sufficient to accurately follow step-function changes over the 1 μs time window of the experiment (no significant signal droop).

2.2.2 Photomultiplier Results.

All shock loading experiments were performed using a fused silica (SiO_2) impactor at a projectile speed of 0.56 mm/μs, corresponding to a peak longitudinal stress of 50 kbar in the Al_2O_3 (and ruby) [10]. Under static conditions, 50 kbar pressure would cause a wavelength shift 1.8 nm [1,2,6].

In order to test for extraneous effects unrelated to the ruby luminescence, one target was made exactly as previously described but without a ruby sample. The target was shocked under conditions identical to those used for the luminescing targets, and Figure 7 shows the oscilloscope record of the net luminescence monitor and the R1/fiducial. The net luminescence monitor detected two increases in light level (decrease in voltage), one being a short pulse (100 ns - probably due to heating of trapped gases between the target and impactor), and the other a gradual increase. Note that the R1/fiducial signal shows only the fiducial step. Thus, while the exact cause of the changes in the net luminescence monitor is not precisely known, they seem to have little or no effect on the R1 line record for a period of hundreds of nanoseconds after the arrival of the optical fiducial.

We next shocked a target with the ruby sample in place. By examining the wave propagation times, and accounting for the known optical path lengths, we determined that the voltage step caused by a wavelength shift should follow the fiducial step by 300 ns. The actual shot record is shown in Figure 8. The fiducial step is followed by a second step after approximately 400 ns. While we do not currently understand this 100 ns discrepancy, the behavior is qualitatively correct. Note that the net luminescence monitor record is similar to that of the test shot, and that only after about 800 ns following the fiducial does a corresponding variation in the R1/fiducial signal occur.

Overall, the PMT experiments have yielded results which are consistent with the expected spectral shift. At the same time, the difficulty in making unambiguous conclusions based on these data emphasizes the fact that more detailed spectral records are needed.

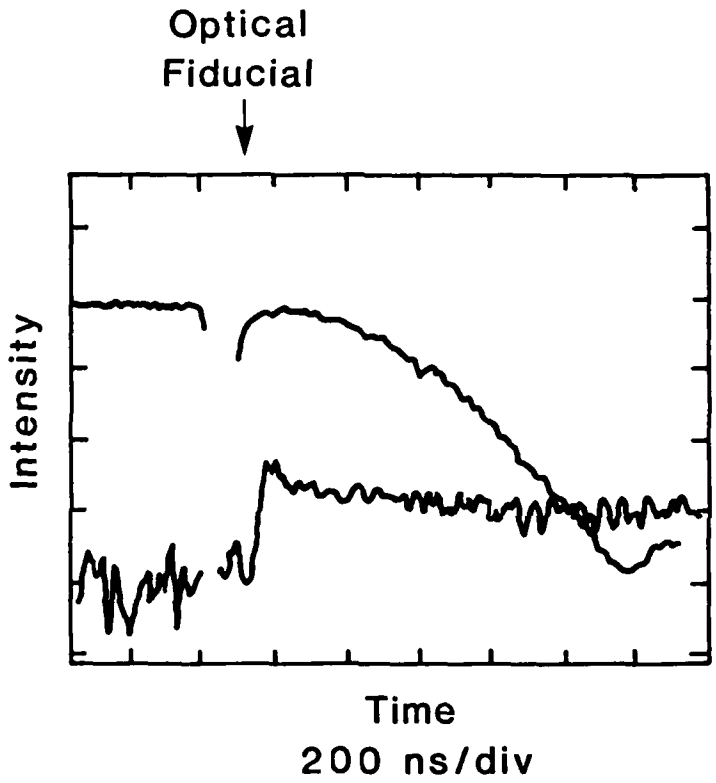

Figure 7. Oscilloscope record of photomultiplier signal. This record was taken during a "trial" experiment with no ruby sample in the target to test for extraneous effects. The upper trace is the net luminescence monitor, the lower trace is the R1/optical fiducial signal. The arrow marks the location of the optical fiducial signal.

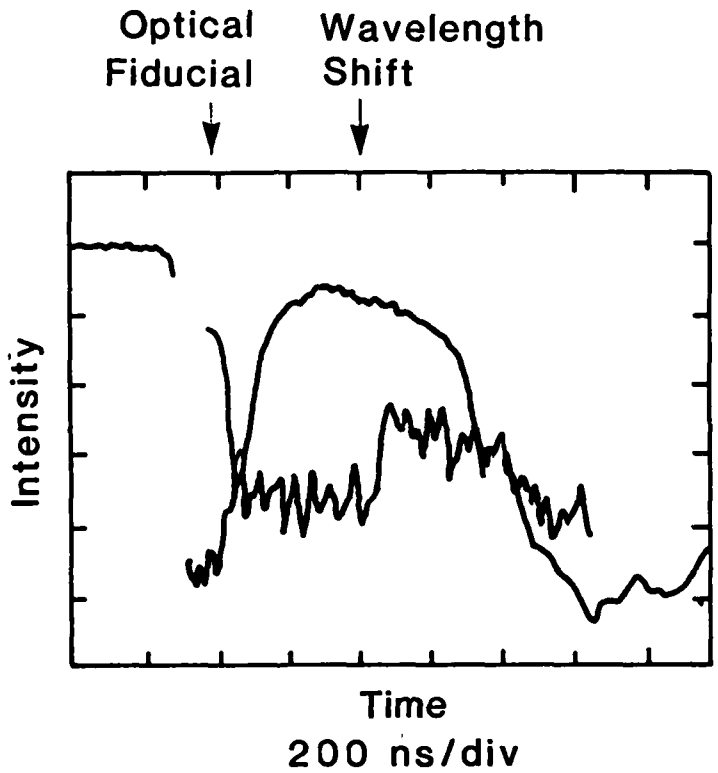

Figure 8. Oscilloscope record of photomultiplier signal during shocking of ruby sample. The upper trace is the net luminescence monitor, the lower trace is the R1/optical fiducial signal. The two arrows indicate the locations of the optical fiducial and the wavelength shift (respectively, from left to right).

2.2.3 Streak Camera Recording.

After gaining some experience using the PMT setup, and obtaining an indication that the ruby luminescence technique is plausible, we considered the use of a streak camera. The apparatus was identical to that used in the PMT tests, except that the PMTs were removed and an electronic streak camera (Cordin model 160) was focused on the image plane of the spectrometer. The image formed by the streak camera was then coupled into an image intensifier (Varo model 6301 microchannel tube), which was placed in direct contact with Polaroid type 57 film. At a streak rate of $5mm/\mu sec$, we were able to obtain a film record which was barely visible to the unaided eye. Two approaches to the resolution of this problem were examined: to raise the level of luminescence reaching the streak camera and/or to increase the recording sensitivity. As a first step, we considered the use of an intensified, two dimensional array target and optical multichannel analyzer to replace film as the recording medium. We obtained the use of such an analyzer (EG&G OMAII and model 1254 Vidicon detector) for a period of two weeks in order to test its effectiveness as a film substitute. Since the Cordin camera has a 50 mm streak length, and the Vidicon detector has only a 12.5 mm active area, we coupled the Vidicon to the Varo image intensifier via a 50 mm to 17 mm tapered fiberoptic bundle (Galileo Electro-Optics) with refractive index matching oil. A good coupling was very difficult to achieve in the time available, so that we were unable to resolve the R1 and R2 lines.

Before discussing the actual shot records, it is helpful to consider the data format of the EG&G OMA Vidicon system. The Vidicon is a 512 x 512 array of picture elements. During exposure, the Vidicon screen accumulates a "charge image" (where the charge at a site is proportional to the integrated light intensity) which is read by a scanning electron beam at a later time. The user defines the scan pattern of the electron beam, and the resultant signal is digitized at 14 bits and stored for later retrieval in the OMA console memory. Because of digitization speed limitations, there is insufficient time after exposure to read all $(512)^2$ elements before leakage from the charge storage sites degrades the image beyond usefulness. The readout scan pattern is made up of units called tracks, each of which is specified by giving a starting point on the screen, a number of elements in

the horizontal direction, and a number of elements in the vertical direction. At each horizontal location, the charge from the specified number of vertical elements is integrated. Each track is thus equivalent to a linear array of specified width and height. In order to avoid leakage from one track to another, a number of cleanup scans are made above and below each track before its readout. This has the effect of severely limiting the number of tracks which can be practically recorded. We were able to record at most 26 tracks. The signal to noise ratio was adjusted by the choice of vertical track height and camera streak rate. We chose a streak rate of 10 mm/μs and a vertical track height of 7 elements, which corresponded to integration over 50 ns (accounting for the tapered fiber bundle and streak rate). The vertical track separation was 20 elements, corresponding to 144 ns from the beginning of one track to the beginning of the next. This means that ruby spectra were recorded at intervals of 144 ns and integrated over 50 ns.

2.2.4 Streak Camera Results.

Two shock experiments were performed under the above conditions, and both gave similar results. Figure 9 is a compressed plot of the 26 tracks (spectra) during a shock experiment, with streak time proceeding from right to left, the streak camera was triggered such that the ruby sample was shocked near the center of the recording time window. A reference streak was recorded immediately before the shot for wavelength calibration. Several features are apparent. First, there was a significant increase in intensity in the vicinity of the shock arrival time. The exact location of that time is unknown because insufficient time was available for the installation of an optical fiducial. Secondly, the intensity dropped over a period of about 500 ns to very near the noise level. Figure 10 is an expanded plot showing five ruby spectra recorded in the vicinity of the shock arrival time, along with the corresponding reference spectra. Note that while the signal-to-noise ratio was very low at the later times, there is definite evidence of a wavelength shifted peak in the last track (leftmost).

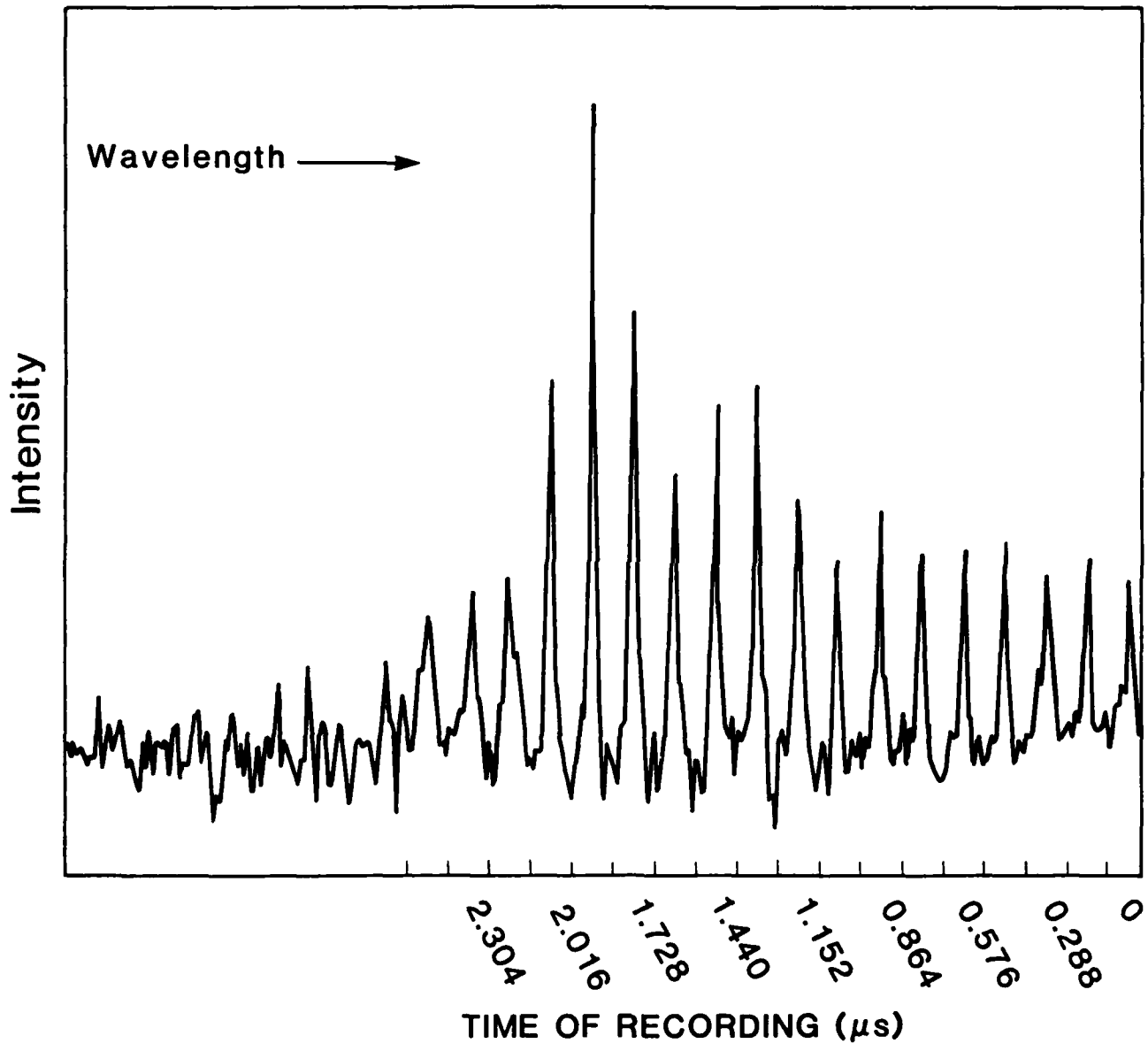

Figure 9. Compressed plot of OMA data showing ruby spectra during a shock experiment. The upper trace is a set of reference spectra taken immediately prior to the shot. At each time indicated, a ruby spectrum was recorded over a period of 50 ns. The shock wave reached the ruby in the vicinity of the center of the plot.

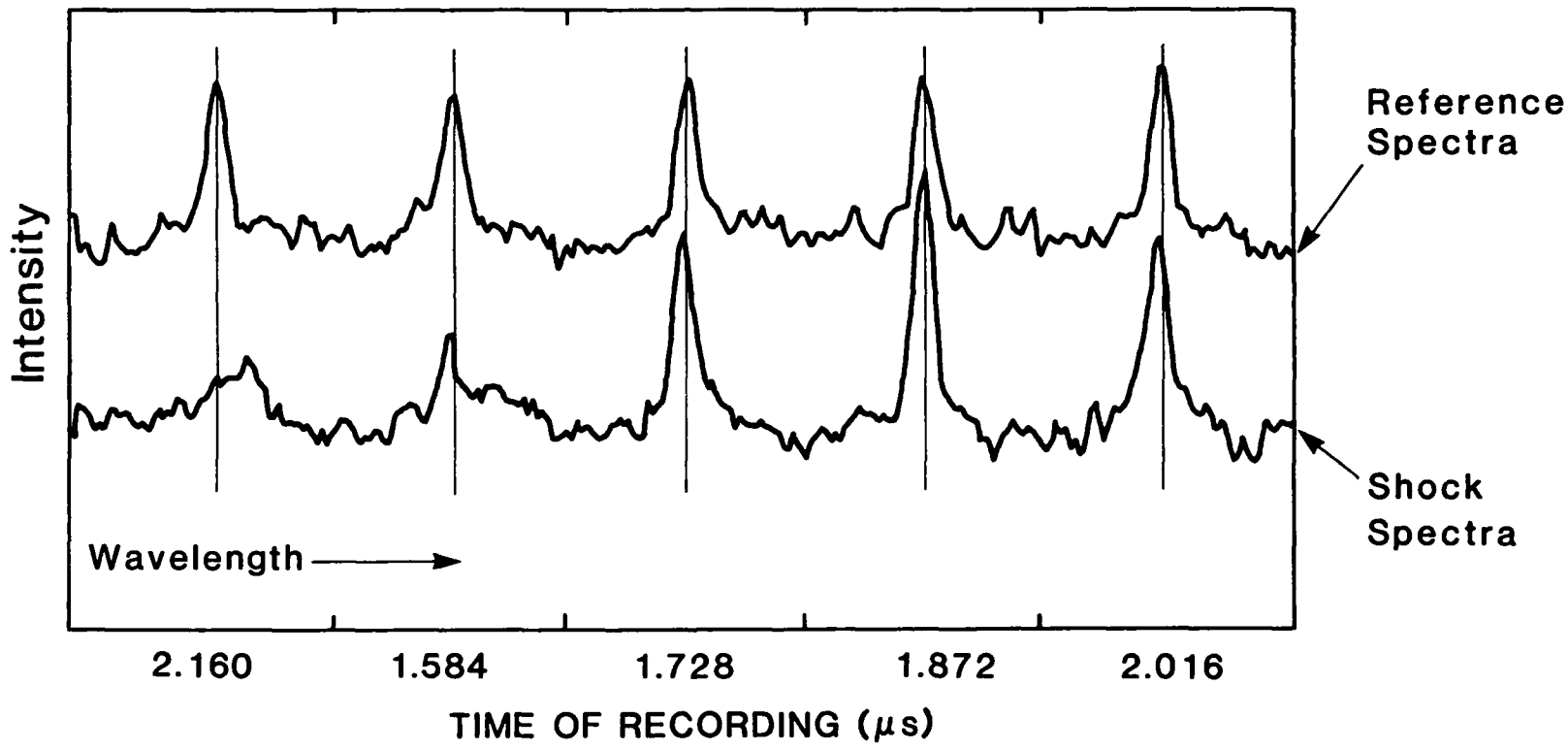

Figure 10. Expanded plot of 5 ruby spectra during a shock experiment (see Figure 9). At each time (from right toleft), the ruby spectrum was recorded for a period of 50 ns. The upper trace is a set of reference spectra taken immediately prior to the shot. Note the wavelength shift in the leftmost spectrum.

As a result of the two shots done with the OMA system, we are confident that a wavelength shift of ruby luminescence has been observed under shock loading. The inability of the OMA II system to provide a continuous temporal record, however, renders it an unsatisfactory replacement for film. While other brands of optical multichannel analyzer may record the entire Vidicon screen, they do so at the expense of intensity resolution (i.e., the number of bits digitized). With these considerations in mind, we feel that the best course at this time is to retain film as the recording medium and to optimize the level of light it receives.

SECTION 3

DISCUSSION

The objective of this preliminary effort has been accomplished. An experimental configuration for the impact experiments has been designed and implemented. The results presented in the last section demonstrate that the R-lines undergo a wavelength shift that is nearly coincident with the shock arrival and propagation through the thin ruby disks. These results are encouraging and demonstrate the feasibility of the overall concept. However, the data are at best qualitative and several changes are required to make quantitative measurements. These changes and improvements in the experiments are indicated next.

3.1 APPARATUS IMPROVEMENTS.

In the early stages of designing the optical system, we calculated and measured the luminescence power and collection efficiency. Details of those calculations are given in Appendix A. We found that we could predict the available luminescence power at the recording device with reasonable accuracy. We have used the calculations as the basis for making a number of apparatus changes designed to optimize the generation, collection, and transmission of luminescence. We will describe these beginning at the film plane and working back along the optical path.

The image intensifier currently used is not gateable and suffers from significant spatial distortion. It should be replaced with a gated, proximity focused, microchannel plate intensifier, which would greatly increase the signal to noise ratio at the film plane while simultaneously removing the spatial distortion inherent in electrostatically focused intensifiers.

The streak camera has F/2 collection optics, but the 0.5 m Jarrel-Ash spectrometer has an effective F-number of greater than F/8. It is thus possible to increase collection efficiency significantly by employing an F/4 spectrometer. We are currently obtaining such a spectrometer (Spex Industries - 1680 Spectramate double spectrometer, 1.8 nm/mm dispersion). Finally, by adding

an electro-optic modulator to the Argon laser system, we can generate a pulsed excitation (about 10 ms) rather than the CW excitation employed to date. This will allow us to use higher excitation powers without sample heating.

There are two changes in target construction that should increase the luminescence collected. The first is to vapor deposit a mirror surface on the impact side of the ruby sample. This would approximately double the laser intensity and the luminescence collection efficiency. The second is to place the optical fiber in direct contact with the ruby sample. Before implementing this change, consideration must be given to the transmission characteristics of optical fiber under shock loading.

3.2 SHOCK LOADING OF OPTICAL FIBER.

We performed three experiments to test the response of hard clad fused silica (Diaguide SMY-UV series) and sapphire (Saphikon) optical fibers to shock loading. These fibers were bonded with epoxy into snug-fitting holes drilled through disks of several materials which acted as supports, then were polished flush with the support disk surface. These were then illuminated by a Xenon flashlamp during impact, while the spectrum of light transmitted though the fiber was recorded by a spectrometer and streak camera. The conclusion was that fused silica fiber can survive a peak pressure of at least 33 kbar with little change in transmission between 350 nm and 700 nm for a time in excess of 1 μsec. The sapphire fiber was subjected to a peak pressure of 90 kbar, and continued transmission for about 280 ns. Our tests indicate that the choice of material in which the fiber is embedded has little effect (the silica fiber performed equally well when surrounded by fused silica and PMMA). The difference in survival time for the two cases may instead be due to the difference in thickness of the supporting layers (i.e. transit time of the shock through the support).

3.3 CONCLUSION.

In summary, we have produced reasonable evidence that the ruby luminescence spectrum can be observed to change under shock conditions. We believe that the apparatus changes listed above will result in a working system for unambiguous measurements of this type. The next goal is to obtain well-defined spectral data using z-cut ruby at ambient and low temperatures, such that the spectral response to shock loading can be quantitatively examined, and the theoretical interpretation of the stress induced wavelength shift can be pursued.

SECTION 4

LIST OF REFERENCES

1. G. J. Piermarini, S. Block, J. D. Barret, and R.A. Forman, "Calibration of the pressure dependence of the R1 ruby fluorescence line to 195 kbar", J. Appl. Phys., 46 , 2774 (1975).

2. D.M. Adams, R. Appleby, and S.K. Sharma, "Spectroscopy at very high pressures: Part X. Use of ruby R-lines in the estimation of pressure at ambient and at low temperatures", J. of Phys. E. Sci., 9 , 1140 (1976).

3. D.E. McCumber and M.D. Sturge, "Linewidth and Temperature Shift of the R lines in Ruby", J. Appl. Phys., 14 , 1682 (196?).

4. Stephanie L. Wunder and Paul E. Schoen, "Pressure measurement at high temperature in the diamond anvil cell", J. Appl. Phys., 52 , 3771 (1981).

5. W. Koechner, "Solid-State Laser Engineering", Springer Series in Optical Sciences, Vol. 1. (New York: Springer-Verlag, 1976), pp. 44-53.

6. T. Hirschfeld, F. Wang, G. Haugen, G. Hieftje, "Fiber Optics Temperature and Pressure Probe", Lawrence Livermore Lab Seminar (private communication).

7. A.L. Schawlow, "Fine Structure and Properties of Chromium Fluorescence in Aluminum and Magnesium Oxide," Advances in Quantum Electronics , J.R. Singer, ed. (New York: Columbia University Press, 1961), pp. 50-64.

8. D.D. Keough and J.Y. Wong, "Variation of the Shock Piezoresistance Coefficient of Manganin as a Function of Deformation", J. Appl. Phys. 41 , 3508 (1970).

9. R.S. Feigelson, W.L. Kway, and R.K. Route, "Single Crystal Fibers by the Laser-Heated Pedestal Growth Method", Opt. Eng. 24 , No. 6, 1102 (1985).

10. L.M. Barker and R.E. Hollenbach, "Shock-Wave Studies of PMMA, Fused Silica, and Sapphire", J. Appl. Phys. 41 , 4208 (1970).

APPENDIX

RUBY LUMINESCENCE EXCITATION AND COLLECTION EFFICIENCY

A.1 LUMINESCENCE POWER CALCULATION.

We considered several excitation sources available to us: flash lamps, a frequency doubled, CW mode locked and Q-switched Nd:YAG laser, and a CW Argon ion laser. We concluded that the Argon laser would be the most efficient source due to the relatively large absorption cross section of ruby at 514.5 nm ($\sigma = 5.8 \times 10^{-20}$ cm^2 [5]) , and the CW nature of the excitation. We note that even though the absorption cross section at the doubled Nd:YAG wavelength (532 nm) is higher than that at the Argon wavelength, the low energy content of the mode-locked and Q-switched pulse train would lead to a much lower excited state population than that generated by the CW Argon laser because the luminescence lifetime is much greater than the Nd:YAG pulse width.

Assuming a sample configuration as shown in Figure 11, we can calculate the luminescence power as follows. A simplified rate equation describing the number density of excited Cr^{3+} ions (n_e) is

$$\frac{dn_e}{dt} = n_g \sigma F - \frac{n_e}{\tau} , \tag{1}$$

where n_g is the density of Cr^{3+} in the unexcited state, σ is the absorption cross section, F is the laser flux (photons/cm^2 second), and τ is the excited state lifetime. We have ignored the fact that the excitation occurs to an intermediate state rather than the luminescing state. This is justified because the decay time from the intermediate to the luminescing state is very short ($\tau \leq 1$ ns)[2]. The excited and unexcited Cr^{3+} densities are related to each other through the total Cr^{3+} density (N) via

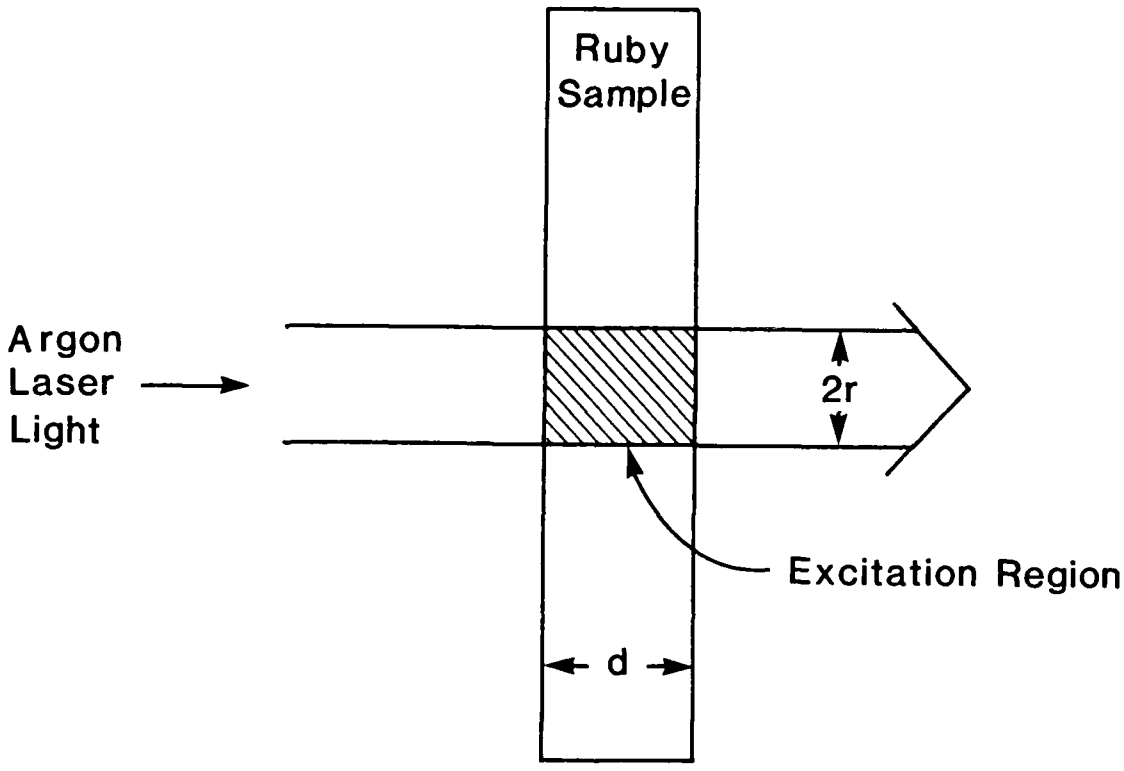

Figure 11. Diagram of geometry used in the calculation of luminescence generation.

$$n_g = N - n_e \,. \tag{2}$$

M

We can thus rewrite Eq. (1) as

$$\frac{dn_e}{dt} = N\sigma F - n_e \left[\sigma F + \frac{1}{\tau} \right] . \tag{3}$$

At this point, we will make the assumption that the laser flux is constant throughout the sample thickness (d), and is spatially uniform in the direction perpendicular to the beam propagation axis. This implies that the fractional loss in laser power must be small, i.e.

$$\frac{\Delta P}{P} = \left[1 - e^{-N\sigma d} \right] << 1 \,. \tag{4}$$

In our case, $N = 1.58 \times 10^{20} cm^{-3}$, $\sigma = 5.8 \times 10^{-20} cm^2$ and $d \leq 7.6 \times 10^{-3}$ cm, so that

$$\frac{\Delta P}{P} \leq 6.7 \; x \; 10^{-2} \,. \tag{5}$$

Since our laser operates in a CW mode, the flux is constant in time. We can therefore simplify Eq. (3) by a change of variables

$$u \equiv n_e - \frac{N\sigma F}{\sigma F + \frac{1}{\tau}} \,. \tag{6}$$

Because N and F are constant,

$$\frac{du}{dt} = \frac{dn_e}{dt} , \tag{7}$$

so that

$$\frac{du}{dt} = -\left(\sigma F + \frac{1}{\tau}\right) u . \tag{8}$$

The solution of Eq. (8) is

$$u(t) = u(t = 0)\, e^{-(\sigma F + \frac{1}{\tau})\, t} . \tag{9}$$

Inserting the initial condition $n_e(0) = 0$, we find the expression for $n_e(t)$ to be

$$n_e(t) = \frac{N\sigma F}{\sigma F + \frac{1}{\tau}} \left(1 - e^{-(\sigma F + \frac{1}{\tau})\, t}\right) . \tag{10}$$

or

$$\frac{n_e(t)}{N} = \frac{1}{1 + (\sigma F \tau)^{-1}} \left(1 - e^{-(\sigma F + \frac{1}{\tau})\, t}\right) . \tag{11}$$

The asymptotic value of n_e/N for $t >> \tau$ is

$$\frac{n_e(t >> \tau)}{N} = \frac{1}{1 + (\sigma F \tau)^{-1}} . \tag{12}$$

The longest time required to reach 95% of the asymptotic value is t = 3τ, i.e. t = 9 ms (let F = 0).

The photon energy for Argon laser light is

$$h\nu = 2.41\ eV = 3.86\ x\ 10^{-19}\ Joules\ . \tag{13}$$

The laser flux is related to laser intensity (I) by

$$F = \frac{I}{h\nu}\ , \tag{14}$$

so that

$$\frac{n(t >> \tau)_e}{N} = \frac{1}{1 + \left(\frac{h\nu}{\sigma I \tau}\right)}\ . \tag{15}$$

Inserting the stated values for σ, τ and $h\nu$, we arrive at

$$\frac{n(t >> \tau)_e}{N} = \frac{1}{1 + \frac{2200}{I}}\ . \tag{16}$$

where I is given in Watts/cm^2.

The total number of excited Cr^{3+} (N_e) is then simply

$$N_e = \left(\pi r^2 d\right) n_e = \frac{\left(\pi r^2 d\right) N}{\left(1 + \frac{2200}{I}\right)}\ . \tag{17}$$

By taking account of the ruby luminescence photon energy ($h\nu = 1.79\,eV = 2.86 \times 10^{-19}\,Joules$), quantum efficiency (0.7, [5]), and lifetime (3 ms), we can calculate the net luminescence power (P_f) as

$$P_f = (h\nu)_{ruby}(0.7)\frac{N_e}{\tau}, \tag{18}$$

or

$$P_f = \left(6.7 \times 10^{-17}\right)\frac{N\pi r^2 d}{1 + \frac{2200}{I}}, \tag{19}$$

where I is given in Watts/cm^2, N is in units of cm^{-3}, and r, d are in cm units. In our work to date, all ruby samples have contained 0.5 percent Cr^{3+} by weight, so that N = 1.58 x $10^{20}\,cm^{-3}$, then

$$P_f = \left(1.1 \times 10^4\right)\left(\pi r^2 \frac{d}{1 + \frac{2200}{I}}\right). \tag{20}$$

Except for variations due to internal reflection at the ruby-air interfaces, this luminescence power should be radiated uniformly into 4π steradians. Equation (20) can be reduced to a more convenient form in the case that $I << 2200\,W/cm^2$, then

$$P_f \approx \left(5cm^{-1}\right)P_l d, \tag{21}$$

where P_l is the laser power incident on the sample, given by

$$P_l = I\left(\pi r^2\right) . \tag{22}$$

It is thus apparent that for low laser intensity, the luminescence power (Equation 20) is nearly independent of the luminescence spot size. We typically use a laser power of 1.5-2 W at the ruby sample.

A.2 FLUORESCENCE COLLECTION.

In order to calculate the luminescence power available for recording after wavelength dispersion, we must now specify the target geometry and the efficiency of the spectrometer. Figure 5 depicts the layout of the target and accompanying optical system. Argon laser light is coupled into a 200 μm core, fused silica fiber (Math Associates QSF-200) via an 80 mm focal length lens. This fiber is approximately 20 m long, and delivers the laser light to a fiberoptic feedthrough on the target chamber. Inside the chamber, this light is transferred to a 600 μm core fiber (QSF-600), which carries it directly to the back of the target. To date, we have succeeded in transmitting approximately 40 percent of the available laser power to the target in this manner. The luminescent spot is 1-2 mm in diameter, and is centered in front of the 1 mm optical fiber (QSF-1000). Because the 1 mm and 600 μm fibers have the same numerical aperature, and are located at about the same distance from the luminescent spot, most of the luminescence striking the 1 mm fiber should be contained.

In order to determine the overall efficiency of the optical system, we examine the individual efficiencies of the 1 mm optical fiber (γ_f), the spectrometer entrance slit (γ_e), the collimating mirror (γ_c), the diffraction grating (γ_g), the focusing mirror (γ_{fm}), and the turning mirror (γ_t). Each of these terms is evaluated next and the results are compared with experimental measurements.

A.2.1 Fiber Collection Efficiency.

The fiber efficiency is approximately determined by the solid angle which it subtends. Defining the fiber diameter by R, and the fiber to ruby distance as r, we have

$$\gamma_f = \frac{1}{2}\left(1-\frac{r}{\sqrt{r^2+R^2}}\right) = 0.015 . \tag{23}$$

This was tested by applying a known laser power, and measuring the luminescence power in the 1 mm fiber with a Fotec C100A power meter. The laser power delivered to the sample was 1.0 W, and the sample thickness was approximately 6.6×10^{-3} cm (0.0026 inches), so that by expression (21)

$$P_f = \frac{1.1 \times 10^4}{2200}(1.0W)(6.6 \times 10^{-3}\, cm) = 3.3 \times 10^{-2} W . \tag{24}$$

Accounting for the calculated collection efficiency, the luminescence power in the 1 mm fiber (P_c) should be

$$P_c = (0.015)P_f = 5.0 \times 10^{-4}\, W . \tag{25}$$

The experimental value was $P_c = 4.4 \times 10^{-4}\, W$. In light of the complex geometry and the approximations made, these values are in good agreement. There is a further loss of 25 percent at the target chamber feedthrough, so that the net fiber collection efficiency as viewed at the spectrometer (γ_{f*}) is

$$\gamma_{f*} = (0.75)\gamma_f = 0.011 . \tag{26}$$

A.2.2 Spectrometer Collection Efficiency.

The optical fiber was placed in direct contact with the spectrometer entrance slit, which had a maximum width of 0.4 mm. The slit height is simply the 1 mm diameter of the optical fiber. The fraction of collected luminescence that passes through the slit is then

$$\gamma_e \approx \frac{(0.4\ mm)(1.0\ mm)}{\pi(0.5\ mm)^2} = 0.5\ . \tag{27}$$

The efficiency of this mirror is given approximately by the ratio of the mirror cross sectional area and the area illuminated by the fiber at the mirror location. The mirror is 5.2 cm square (i.e., has an area of 27 cm^2). The optical fiber has a numerical aperature of 0.4, so that the luminescence emerges in a light cone of half-angle (θ)

$$\theta = \sin^{-1}(0.4) = 24^o\ . \tag{28}$$

The area defined by angle θ and the 50 cm focal length of the spectrometer (0.5 m Jarrel-Ash) is

$$A = \pi[(50\ cm)\tan\theta]^2 = 1500\ cm^2\ . \tag{29}$$

Taking into account the 90 percent reflectivity of the aluminum coating, the mirror has an efficiency of

$$\gamma_e = (0.9)\left(\frac{27}{1500}\right) = 0.016\ . \tag{30}$$

The 1180 groove/mm, ruled grating was blazed for 500 nm. Extrapolation of the grating specifications yields an efficiency of about 66 percent at 700 nm. We estimate a further loss of 32 percent due to vignetting of the grating at the 694.3 nm setting. The grating efficiency is then

$$\gamma_g = (0.66)(0.68) = 0.45\ . \tag{31}$$

The focusing and turning mirrors each have about 90 percent efficiency (aluminum), so the spectrometer efficiency is

$$\gamma_s = \gamma_e \gamma_c \gamma_g \gamma_{fm} \gamma_t$$

$$= (0.5)(0.016)(0.45)(0.9)(0.9) = 2.9 \; x \; 10^{-3} . \tag{32}$$

A.2.3 System Collection Efficiency.

The combined fiber/spectrometer efficiency is

$$\gamma = \gamma_{fs} \gamma_s = 3.2 \; x \; ^{-5} . \tag{33}$$

The spectrally dispersed luminescence power P_d is then given in terms of the net luminescence power at the sample as

$$P_d = \gamma P_f , \tag{34}$$

and is divided between the R1 and R2 lines in the ratio $P_d(R1)/P_d(R2) = 1.5$ at room temperature.

This was tested by collecting a portion of the R1 line with a 600 μm fiber, which was placed at the exit plane of the spectrometer, and determining the luminescence power by using the Fotec power meter. Since the spectrometer has a magnification of 1, the area covered by the R1 line at the exit plane was equal to that of the entrance slit, 0.4 mm^2 (this is because the product of slit width and dispersion is greater than the spectral line width). We thus collected (portion of the 1mm x 0.4 mm area falling on the 0.6 mm diameter fiber)

DISTRIBUTION LIST

DEPARTMENT OF DEFENSE

DEFENSE ADVANCED RSCH PROJ AGENCY
ATTN: DIRECTOR

DEFENSE INTELLIGENCE AGENCY
ATTN: RTS-2B

DEFENSE NUCLEAR AGENCY
ATTN: RAEV
ATTN: SPAS
ATTN: SPSS
12 CYS ATTN: SPTD
ATTN: STNA
ATTN: STRA
ATTN: STSP
4 CYS ATTN: STTI-CA

DEFENSE TECHNICAL INFORMATION CENTER
12 CYS ATTN: DD

DEPT OF DEFENSE EXPLO SAFETY BOARD
ATTN: CHAIRMAN

FIELD COMMAND DNA DET 2
LAWRENCE LIVERMORE NATIONAL LAB
ATTN: FC-1

FIELD COMMAND DEFENSE NUCLEAR AGENCY
ATTN: FCT
ATTN: FCTEI
ATTN: FCTT

FIELD COMMAND TEST DIRECTORATE
ATTN: FCTC

NATIONAL SECURITY AGENCY
ATTN: DIRECTOR

UNDER SECY OF DEF FOR RSCH & ENGRG
ATTN: STRAT & SPACE SYS (OS)

DEPARTMENT OF THE ARMY

HARRY DIAMOND LABORATORIES
ATTN: C KENYON
ATTN: HD-NW-P J MESZAROS 20240
ATTN: M BUSHELL
ATTN: R GRAY
ATTN: SLCHD-NW-R J BLACKBURN 22000
ATTN: SLCHD-NW-R J VANDERWALL 22800
ATTN: SLCHD-NW-RH G MERKEL
ATTN: SLCHD-NW-RH R GILBERT 22800

U S ARMY ATMOSPHERIC SCIENCES LAB
ATTN: SLCAS-D COMMANDER/DIR

U S ARMY BALLISTIC RESEARCH LAB
ATTN: SLCBR-TB-E P HOWE

U S ARMY COLD REGION RES ENGR LAB
ATTN: TECHNICAL DIRECTOR

U S ARMY COMMUNICATIONS R&D COMMAND
ATTN: COMMANDER

U S ARMY ELECTRONICS R & D COMMAND
ATTN: DELET-ER
ATTN: DRSL

U S ARMY ENGINEER DIV HUNTSVILLE
ATTN: COMMANDER

U S ARMY ENGR WATERWAYS EXPER STATION
ATTN: G P BONNER WESJV-Z
ATTN: J INGRAM WESSER
ATTN: R WELCH WESSE-R
ATTN: R WHALIN WESZT
ATTN: WESSE

U S ARMY STRATEGIC DEFENSE CMD
ATTN: DASD-PP

U S ARMY STRATEGIC DEFENSE CMD
ATTN: BMDSC-HW R DEKALB
ATTN: DASD-H-SAV R C WEBB

U S ARMY STRATEGIC DEFENSE COMMAND
ATTN: ATC
ATTN: ATC-O F HOKE

USA ELECT WARFARE/SEC,SURV & TARGET ACQ CTR
ATTN: AMSEL-EW-SS S KRONENBERG

DEPARTMENT OF THE NAVY

DAVID TAYLOR NAVAL SHIP R & D CTR
ATTN: CODE 1
ATTN: CODE 174

NAVAL SURFACE WEAPONS CENTER
ATTN: J FORBES R-13
ATTN: R TUSSING R-15

NAVAL WEAPONS CENTER
ATTN: G GREENE

DEPARTMENT OF THE NAVY (CONTINUED)

NAVAL WEAPONS EVALUATION FACILITY
ATTN: CLASSIFIED LIBRARY

OFFICE OF NAVAL TECHNOLOGY
ATTN: CODE 217

DEPARTMENT OF THE AIR FORCE

AIR FORCE ARMAMENT LABORATORY
ATTN: M ZIMMER

AIR FORCE OFFICE OF SCIENTIFIC RSCH
ATTN: AFOSR/NA

AIR FORCE WEAPONS LABORATORY, AFSC
ATTN: NTCO C AEBY
ATTN: NTED D COLE
ATTN: NTED E SEUSY
ATTN: NTED J RENICK
ATTN: NTEO

BALLISTIC MISSILE OFFICE/DAA
ATTN: ENSN

DEPARTMENT OF ENERGY

DEPARTMENT OF ENERGY
ATTN: DIRECTOR, OSPA

EG&G ENERGY MEASUREMENTS
ATTN: W R KITCHEN

EG&G IDAHO INC
ATTN: J EPSTEIN

UNIVERSITY OF CALIFORNIA
LAWRENCE LIVERMORE NATIONAL LAB
ATTN: B BOWMAN
ATTN: E LEE
ATTN: G E VOGTLIN
ATTN: L-10 W E FARLEY
ATTN: W A BOOKLESS

LOS ALAMOS NATIONAL LABORATORY
ATTN: C S YOUNG P-14
ATTN: D EILERS
ATTN: DIRECTOR
ATTN: G BARRASCH
ATTN: G M SMITH
ATTN: J OGLE P-14
ATTN: J TOEVS P-14
ATTN: M PONGRATZ
ATTN: M WILKE
ATTN: S STONE P-14
ATTN: T MCKOWN

OAK RIDGE NATIONAL LABORATORY
ATTN: D BARTINE
ATTN: DIRECTOR
ATTN: R L ANDERSON

SANDIA NATIONAL LABORATORIES
ATTN: DIV 7111 B VORTMAN
ATTN: ORG 7116 C W COOK
ATTN: ORG 7116 S R DOLCE
ATTN: 7112 C W SMITH

OTHER GOVERNMENT

DEPARTMENT OF COMMERCE
ATTN: SEC OFC FOR INSTR DIV
ATTN: SEC OFC FOR O PETERSONS
ATTN: SEC OFC FOR OFFICE OF DIRECTOR
ATTN: SEC OFC FOR R H MCKNIGHT

FEDERAL EMERGENCY MANAGEMENT AGENCY
ATTN: OFC OF RSCH/NP H TOVEY

NATIONAL BUREAU OF STANDARDS
ATTN: A BURR
ATTN: M BROADHURST
ATTN: R E LAWTON

DEPARTMENT OF DEFENSE CONTRACTORS

ACUREX CORP
ATTN: PRESIDENT W DEAN

ADVANCED RESEARCH & APPLICATIONS CORP
ATTN: J STANLEY
ATTN: M BOYLE
ATTN: R ARMISTEAD

APPLIED RESEARCH ASSOCIATES, INC
ATTN: N HIGGINS

APTEK, INC
ATTN: T MEAGHER

ASTRON RESEARCH & ENGINEERING
ATTN: J HUNTINGTON

BDM CORP
ATTN: B BENDOW

CALIFORNIA RESEARCH & TECHNOLOGY, INC
ATTN: K KREYENHAGEN
ATTN: M ROSENBLATT
ATTN: S SCHUSTER

CALIFORNIA RESEARCH & TECHNOLOGY, INC
ATTN: F SAUER

CALSPAN CORP
ATTN: PRESIDENT

CARPENTER RESEARCH CORP
ATTN: H J CARPENTER

CHARLES STARK DRAPER LAB, INC
ATTN: P KELLY

DEPT OF DEFENSE CONTRACTORS (CONTINUED)

CUSHING ASSOCIATES, INC
ATTN: V CUSHING

DEVELCO, INC
ATTN: PRESIDENT

ECTRON CORP
ATTN: E CUNNINGHAM

EG&G WASH ANALYTICAL SVCS CTR, INC
ATTN: A BONHAM
ATTN: G SOWER
ATTN: M GRUCHALLA

EG&G/KIRTLAND
ATTN: S ORRELL

EG&G, INC
ATTN: E C SHIVERS
ATTN: L F SANDOVAL
ATTN: N F COCHRANE
ATTN: P A ZAGARINO
ATTN: R D SENO

FORD AEROSPACE & COMMUNICATIONS CORP
ATTN: PRESIDENT

G B LABORATORY, INC
ATTN: G BURGHART

GENERAL RESEARCH CORP
ATTN: E STEELE
ATTN: R GLOBUS

GEO CENTERS, INC
ATTN: E MARRAM
ATTN: H LINNERUD

GEOSCIENCE LTD
ATTN: DR H POPPENDIEK

H-TECH LABS, INC
ATTN: B HARTENBAUM

HTL K WEST
ATTN: A D GOEDEKE

IIT RESEARCH INSTITUTE
ATTN: DIRECTOR

JAYCOR
ATTN: R STAHL

JAYCOR
ATTN: R BONN

JAYCOR
ATTN: PRESIDENT

KAMAN SCIENCES CORP
ATTN: B TAYLOR
ATTN: C HUDSON
ATTN: D ELDER
ATTN: D OSBORN
ATTN: E COLE
ATTN: F RICH
ATTN: G ROARK
ATTN: N KOOZER

KAMAN SCIENCES CORP
ATTN: E CONRAD

KAMAN TEMPO
ATTN: DASIAC

KAMAN TEMPO
ATTN: DASIAC

LOS ALAMOS TECHNICAL ASSOCIATES, INC
ATTN: PRESIDENT

M I T LINCOLN LAB
ATTN: DR. R SLATTERY

MITRE CORP
ATTN: J E DRIVER

NEW MEXICO ENGINEERING RESEARCH INSTITUTE
ATTN: DIRECTOR

PACIFIC-SIERRA RESEARCH CORP
ATTN: H BRODE, CHAIRMAN SAGE
ATTN: R SMALL

PACIFIC-SIERRA RESEARCH CORP
ATTN: G MCLELLAN

PACIFICA TECHNOLOGY
ATTN: R ALLEN

PHYSICAL DYNAMICS, INC
ATTN: B KREISS

PHYSICS APPLICATIONS, INC
ATTN: DOCUMENT CONTROL

PHYSICS INTERNATIONAL CO
ATTN: G MANKINEN
ATTN: P CAYERE
ATTN: R Z CONROW

R & D ASSOCIATES
ATTN: C K B LEE
ATTN: D HOLLIDAY
ATTN: D SIMONS
ATTN: F A FIELD
ATTN: J LEWIS

DEPT OF DEFENSE CONTRACTORS (CONTINUED)

RAND CORP
ATTN: P DAVIS

RAND CORP
ATTN: B BENNETT

RAYTHEON CO
ATTN: J WECKBACK

RIVERSIDE RESEARCH INSTITUTE
ATTN: PRESIDENT

S-CUBED
ATTN: C PETERSEN
ATTN: D GRINE
ATTN: P COLEMAN

SCIENCE & ENGRG ASSOCIATES, INC
ATTN: J CRAMER

SCIENCE & ENGRG ASSOCIATES, INC
ATTN: J STOCKTON
ATTN: R BEATY

SCIENCE APPLICATIONS INTL CORP
ATTN: K SITES
ATTN: L A MILLONZI

SCIENCE APPLICATIONS INTL CORP
ATTN: L SCOTT
ATTN: R SCHLAUG

SCIENCE APPLICATIONS INTL CORP
ATTN: B GORDON
ATTN: E TOTON
ATTN: S METH

SCIENCE APPLICATIONS INTL CORP
ATTN: V J ORPHAN

SRI INTERNATIONAL
ATTN: D KEOUGH
ATTN: E VANCE
ATTN: P DE CARLI

TELEDYNE BROWN ENGINEERING
ATTN: PRESIDENT

WASHINGTON STATE UNIVERSITY
2 CYS ATTN: P HORN
2 CYS ATTN: PROF G DUVALL
2 CYS ATTN: PROF Y GUPTA

FOREIGN

ATOMIC WEAPONS RESEARCH ESTABLISHMENT
ATTN: J BALDERSTON

AUSTRALIA EMBASSY
ATTN: OFC OF THE DEF SCI ATTACHE

BRITISH DEFENCE STAFF
ATTN: ACOW S MITCHELL

DEFENSE RESEARCH ESTABLISHMENT
ATTN: DR J ANDERSON
ATTN: I MOEN

DEFENSE TECH & PROCUREMENT GROUP
ATTN: B ANET

ERNST-MACH-INSTITUT
ATTN: H REICHENBACH

FEDERAL INSTITUTE OF TECHNOLOGY
ATTN: DR J STUDER

ISRAEL EMBASSY
ATTN: OFC OF THE MIL ATTACHE

NATIONAL DEFENCE RESEARCH INSTITUTE
ATTN: H AXELSSON
ATTN: H GORAN

NORWEGIAN EMBASSY
ATTN: MILITARY ATTACHE

ROYAL NETHERLANDS EMBASSY
ATTN: MILITARY ATTACHE

SWEDISH EMBASSY
ATTN: ASSISTANT ARMY ATTACHE

TECHNOLOGISCH LABORATORIUM (TNO)
ATTN: DIRECTOR

END

11-86

DTIC